

Accepted Manuscript

Title: Facile electrochemical synthesis of anatase nano-architected titanium dioxide films with reversible superhydrophilic behavior

Author: Saurav Sorcar Abdul Razzaq Haining Tian Craig A. Grimes Su-Il In



PII: S1226-086X(16)30411-7
DOI: <http://dx.doi.org/doi:10.1016/j.jiec.2016.10.032>
Reference: JIEC 3144

To appear in:

Received date: 18-7-2016
Revised date: 21-10-2016
Accepted date: 23-10-2016

Please cite this article as: S. Sorcar, A. Razzaq, H. Tian, C.A. Grimes, S.-I. In, Facile electrochemical synthesis of anatase nano-architected titanium dioxide films with reversible superhydrophilic behavior, *Journal of Industrial and Engineering Chemistry* (2016), <http://dx.doi.org/10.1016/j.jiec.2016.10.032>

This is a PDF file of an unedited manuscript that has been accepted for publication. As a service to our customers we are providing this early version of the manuscript. The manuscript will undergo copyediting, typesetting, and review of the resulting proof before it is published in its final form. Please note that during the production process errors may be discovered which could affect the content, and all legal disclaimers that apply to the journal pertain.

1 **Facile electrochemical synthesis of anatase nano-architected**
2 **titanium dioxide films with reversible superhydrophilic behavior**

3
4 Saurav Sorcar^a, Abdul Razzaq^a, Haining Tian^b, Craig A. Grimes^c and Su-II In^{a*}

5 ^a *Department of Energy Systems Engineering, DGIST, 50-1, Sang-ri, Hyeonpung-myeon, Dalseong Gun,*
6 *Daegu-711-873, Republic of Korea.*

7
8 ^b *Physical Chemistry, Department of Chemistry-Ångström Laboratory, Uppsala University, Box 523, Uppsala SE*
9 *75120, Sweden.*

10
11 ^c *Flux Photon Corporation, 116 Donmoor Court, Garner, North Carolina, 27529, United States.*

12
13 * **Corresponding Author: Tel: +82-53-785-6417; Fax: +82-53-785-6409**

14 **E-mail address: * insuil@dgist.ac.kr**

15 **Abstract**

16 In the present work we report a facile and readily-scalable electrochemical
17 anodization technique for preparation of superhydrophilic TiO₂ surfaces having reversible
18 wettability properties. The electrochemically anodized Ti foils manifest nanoscale
19 topographical features, interconnected nanowebs and nanofibrils, that enhance both surface
20 roughness and light absorption. After 5 minutes of UV illumination a water contact angle
21 (WCA) of 4.8° is measured for a 5 μL de-ionized water droplet, while after 5 minutes of
22 white-light illumination the WCA is 3.2°. Moreover, under UV illumination the
23 superhydrophilic Ti foils exhibit self-cleaning properties. Key factors contributing to the
24 superhydrophilic character include surface topology, and surface chemical reactions.

25
26 **Keywords:** Electrochemical anodization; superhydrophilic; nanowebs; nanofibrils; titanium
27 dioxide; surface topology.

28 1. Introduction

29 Wettability is a fundamental surface property[1–3]. The pioneering efforts of Wenzel
30 and co-workers[4], and so too Cassie and co-workers[5], demonstrated that surface free
31 energy and surface topologies play pivotal roles in governing surface wettability[6].
32 Hydrophilic metal surfaces are of significant interest to the scientific and industrial
33 communities since they offer a means to promote adhesion as well as biocompatibility[7,8].
34 Within the range of available metals Ti is extensively used for medical implants due to its
35 strength, excellent corrosion resistance, biocompatibility, and osseointegration properties[9].
36 Titanium dioxide surfaces that when illuminated by sunlight become superhydrophilic,
37 having a contact angle less than 10° [10], were discovered in 1995 with, subsequently,
38 commercial application to car-door mirrors[11], exterior building coatings[11], and self-
39 cleaning glass[11]. Presently, Ti-based materials possessing hydrophilic surfaces are
40 generally realized through surface treatments that include chemical or mechanical surface
41 roughening[9,12]. Previous reports on synthesis of hydrophilic TiO_2 surfaces via anodic
42 oxidation include fabrication of hydrophilic TiO_2 nanotubes arrays on titanium foil by which
43 a water contact angle of approximately 28° [13], as well as diameter-sensitive
44 hydrophilicity[14]. Wu *et al* report thin-film Bragg stacks composed of TiO_2
45 nanoparticles[15]. Recently, superhydrophilic TiO_2 surfaces have been reported by
46 fabrication techniques that include direct current glow discharge plasma[16], and
47 femtosecond UV pulses[17]. Tugulu and co-workers[9] successfully prepared
48 superhydrophilic surfaces on a Ti implant through a multistep process that includes
49 sandblasting, thermal acid etching, and alkali treatment, while Hoshian *et al* report a photo-
50 switchable TiO_2 architecture synthesized through the use of atomic layer deposition
51 (ALD)[18]. Yet for all the excellent research that has been done, we believe there remains an
52 unmet need to develop improved methods for preparing superhydrophilic surfaces on

53 titanium. To that end, our interest is in the use of electrochemical anodization, a low cost
54 readily-scalable synthesis route by which a variety of nanoscale topologies can be easily
55 achieved, to alter Ti surfaces by which surface wettability can be controlled[19–25].

56 A crucial matter in determining practical application of superhydrophilic surfaces is
57 durability of the surface wettability, a factor of intrinsic surface properties as well as the
58 ambient environment[26–28]. In practical applications the original wettability of the surface
59 is easily lost due to adsorption of organic molecules[29], however on TiO₂-related materials
60 such contaminants can be photocatalytically decomposed[30,31]

61 While challenges such as fragility, agglomeration in the case of P25 powders, and
62 device-scalability [32,33] often limit commercial application of superhydrophilic Ti surfaces,
63 electrochemical anodization offers the opportunity for *in-situ* preparation of superhydrophilic
64 Ti surfaces with self-cleaning capabilities, thus attaining a durable superhydrophilicity.
65 However, previous reports on the synthesis of TiO₂ nanostructures using electrochemical
66 anodization have utilized highly acidic [34,35] and/or fluoride containing electrolytes[36,37]
67 that, often enough, preclude many applications.

68 Motivated from the limitations mentioned above, herein we detail a simple, less toxic,
69 inexpensive and readily scalable method to produce superhydrophilic surfaces on Ti foil
70 substrates by constant current electrochemical anodization using a sodium hydroxide (NaOH)
71 electrolyte. The superhydrophilic properties imparted to the anodized Ti foils are ascribed to
72 the generation of a titanium oxide surface coating comprised of a well-defined interconnected
73 nanofibrils network that offers enhanced surface roughness combined with improved light
74 absorption. The wetting durability of the electrochemically anodized Ti foils are studied to
75 check the reproducibility of the initial surface state, and the photocatalytic removal of organic
76 contaminants demonstrated. We believe our work will help lead to more cost-effective, high

77 performance superhydrophilic surfaces for both medical and industrial applications with
78 enhanced durability and reversibility in their surface wetting properties.

79

80 **2. Experimental**

81 2.1 Materials

82 Titanium foils (0.1 mm in thickness, 99.5%) from Nilaco Corporation, Japan were
83 used in this investigation. Sodium hydroxide was purchased from Duksan Pure Chemicals
84 Co. Ltd. Korea. Deionized (DI) water was used throughout all experiments.

85

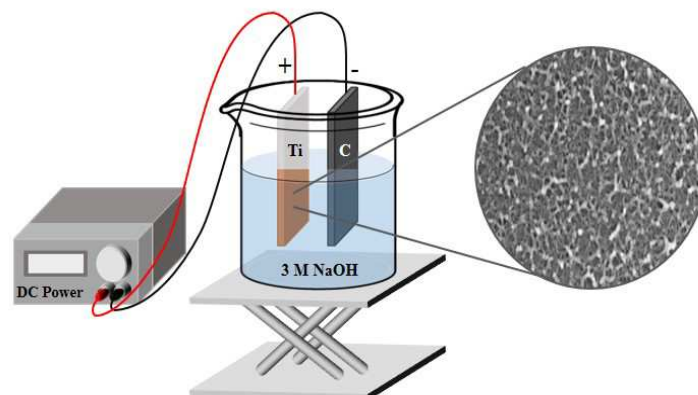
86 2.2 Electrochemical synthesis of interconnected nanofibril films upon Ti foils.

87 Films comprised of interconnected nanofibrils were synthesized upon Ti foil
88 substrates by constant current electrochemical anodization using a NaOH-based alkaline
89 electrolyte. Prior to anodization the Ti foils (2 x 1 cm) were sequentially washed, using
90 ultrasonication, in acetone, ethanol, and distilled water, and then dried in a stream of nitrogen
91 gas. All anodization experiments were carried out at room temperature using a standard two-
92 electrode arrangement with the Ti foil serving as the anode, and carbon paper (2 x 1 cm)
93 serving as the cathode. Both electrodes, separated by a distance of 3 cm, were placed in a
94 polypropylene beaker containing 3M NaOH. Anodization was carried out using a
95 programmable DC power supply (OPE-S Series). Different samples were prepared by
96 varying the applied current, with an anodization duration of 30 minute for each Ti foil
97 sample. The samples were named as Ti-X, where X = 10, 20, 30, 40 and 50 corresponding to
98 10mA, 20mA, 30mA, 40mA and 50mA anodization current, respectively. After anodization
99 the Ti foils were immersed in 0.05M HCl for one hour to exchange the Na⁺ ions with H⁺ ions.
100 Finally, the anodized Ti-X foils were washed with a copious amount of DI water, allowed to
101 dry under ambient conditions, then annealed at 350°C for 1 hour (tube furnace under an air

102 flow of $30 \text{ cm}^3/\text{min}$), to obtain oxygen related surface defects known to form weak bonds
103 with water molecules thus enhancing hydrophilic properties [38]. **Fig. 1** presents the
104 experimental setup used for electrochemical anodization of the Ti foils.

105

106



107

108

109

110 **Fig. 1.** Schematic illustration showing the electrochemical anodization of Ti foils.

111

112

113 2.3 Characterization

114 The morphology of the anodized Ti foils were examined using a field emission
115 scanning electron microscope (FE-SEM, Hitachi F-4800) with an accelerating voltage of
116 3 kV. Crystallographic properties were determined by use of X-ray diffractometry (XRD);
117 Panalytical, Empyrean, operating at 40 kV and 30 mA with Cu $K\alpha$ radiation ($\lambda=1.54\text{\AA}$) as an
118 X-ray source, scanned at $0.02^\circ/\text{min}$ in the range of $2\theta=20^\circ-80^\circ$. Surface composition and
119 oxidation states were determined by X-ray photoelectron spectroscopy (XPS), Thermo VG,
120 K-alpha, using the Al $K\alpha$ line (148606 eV) as the X-ray source. UV-visible diffuse
121 reflectance spectroscopy (DRS) of the materials were measured using a Cary series UV-
122 visible near IR spectrophotometer with a diffuse reflection accessory.

123 Surface roughness was evaluated by atomic force microscopy (AFM); Park systems
124 XE7, in the non-contact mode using conventional silicon nitride cantilevers under ambient
125 conditions (i.e. 295 K, relative humidity 50%, air). The AFM scan area of each sample was
126 $5\ \mu\text{m} \times 5\ \mu\text{m}$ at a scan rate of 0.2 Hz. In accordance with literature [39-43], each sample was
127 measured at five different positions to obtain a mean value of the RMS roughness (R_{rms}).

128

129 2.4 Water contact angle (WCA) measurements

130 Deionized water was employed as the source for static sessile WCA measurements.
131 The wetting properties of water droplets on the sample surfaces were characterized using an
132 optical contact-angle system (Krüss DSA 100, Germany); experimental error in the
133 measurements was $\pm 3^\circ$. Initial WCA measurements were performed in a dark room. For the
134 WCA studies after UV light illumination, a 6 W handheld UV light lamp ($\lambda = 365\ \text{nm}$) was
135 used and the resulting WCA measured after 5 minutes of illumination. Similarly, a 10 W
136 white light with a color temperature of 3000 K, manufactured by Sigma Luminous, was used
137 to check the WCA under indoor light conditions, the spectrum of which has been provided in
138 the supplementary information. WCA values were measured by dispensing water droplets at
139 five different positions for each of three different samples prepared using a given anodization
140 condition. All data was exported into Excel (Microsoft, USA) spreadsheets for analysis.
141 Data can be found in **Tables S2 to S5**.

142

143 2.5 Self- cleaning experiments

144 A dipping method was used to apply oleic acid, used as our test contaminant [44,45].
145 The samples were immersed in an acetone solution of 1wt% oleic acid for 30 minutes and
146 then placed in a vacuum oven at 50°C for 15 minutes. The oleic acid contaminated samples
147 were then UV illuminated with the WCA measured at specific intervals. In accordance with

148 literature [45,46,75], standard errors and standard deviations were obtained by measuring the
149 WCA at five different positions upon a single sample.

150

151 2.6 Reproducibility of the initial surface state

152 The WCA was first measured for the samples while in the dark. The samples were
153 then exposed either to UV or white light illumination, and the WCA again measured. To re-
154 obtain the less hydrophilic surface state the samples were dipped in DI water and kept in a
155 vacuum oven at 100°C for 30 minutes. This was followed by WCA measurements in the
156 same order: dark; then either UV or white light illumination. Using the same samples this
157 cycle was repeated several times to confirm reproducibility of the initial surface state. One
158 should note that for each condition the presented WCA values are obtained from the average
159 WCA values of three different samples with WCA measured at five different positions upon
160 the sample, a total of fifteen WCA measurements. In accordance with literature [47,48],
161 these values are exported to Excel (Microsoft, USA) for analysis and plotting of standard
162 error bars. Data can be found in **Tables S6 to S9**.

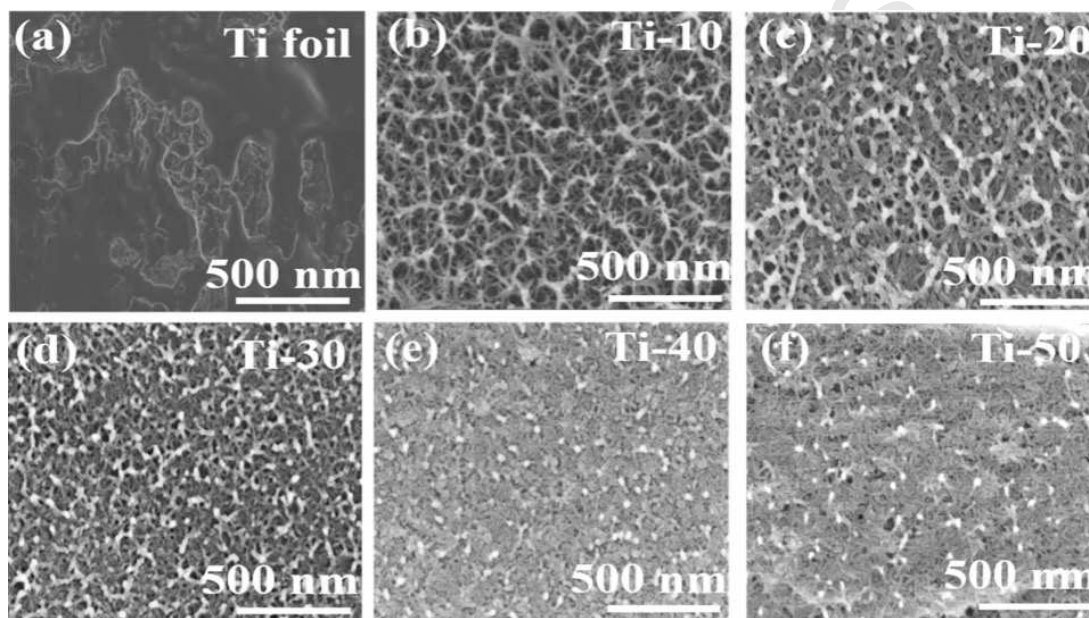
163

164 3. Results and discussion

165 **Fig. 2** shows FESEM images of the Ti foils before and after anodization at applied
166 currents ranging from 10 mA to 50 mA. As seen in **Fig. 2(a)**, the initial Ti foil surface is
167 without any well-defined morphology. In electrolytes of high NaOH concentration a particle-
168 like morphology is observed upon the anodized Ti foil surface, as seen in **Fig. S1 (a) and (b)**.
169 Similarly, anodization of longer duration, **Fig. S1(c)**, resulted in but cracks over the Ti foil
170 surface without any well-defined morphology. The reason behind these non-uniform film
171 generation has been reported earlier[49]; according to Prusi, *et al*, electrolytes possessing
172 high alkalinity possess extreme solvent action characteristics, thus yielding inhomogeneous

173 films of poor adhesion over the Ti foil surface[41]. It is observed for the 10 mA anodized
174 sample, **Fig. 2(b)**, that an interconnected nanoweb surface morphology is achieved. With an
175 increase in the applied current to 20 mA, **Fig. 2(c)**, one sees a transition from a network of
176 interconnected nanowebs to that of a nanofibrils network of moderate density. No change in
177 morphology is noticed with the applied current increasing from 20 mA up to 50 mA, only an
178 increase in the density of the nanofibrils.

179



180

181 **Fig. 2.** FE-SEM images of (a) Ti foil, (b) Ti-10, (c) Ti-20, (d) Ti-30, (d) Ti-40, and (d) Ti-50.

182

183 It has previously been reported that Ti anodization initially starts in the form of point
184 etching[50,51]. Titanium possesses an innate oxide barrier layer on its surface, which in the
185 presence of an alkaline medium locally dissolves [24, 40,43]; the self-formed films in the
186 beginning consist mostly of $\text{Ti}(\text{OH})_4$ (Reaction 1 and 2). Etching begins by pitting of the
187 oxide layer, which provides the least resistive route for the current. Once such pits form,
188 etching proceeds longitudinally to the interior to form new, smaller, pit-like structures, while
189 also proceeding laterally to etch the formed walls by which the nanoweb network appears.

190 As the current increases, the balance between field-assisted chemical dissolution and
 191 oxidation changes which also increases the film thickness (**Fig. S1**). $\text{Ti}(\text{OH})_4$ then converts to
 192 hydrated oxide $\text{TiO}_{2-x}(\text{OH})_{2-x}$ (Reaction 3), followed by formation of the nanoweb/nanofibril
 193 morphology over the Ti foil surface. Annealing of the hydrated oxide $\text{TiO}_{2-x}(\text{OH})_{2-x}$ gives rise
 194 to the anatase phase (Reaction 4). The electrochemical oxide growth is a redox reaction at the
 195 oxide/electrolyte interface, as shown below[49,52,53]:

196

- 197 1. $\text{Ti} \rightarrow \text{Ti}^{+4} + 4\text{e}^-$
- 198 2. $\text{Ti}^{+4} + 4\text{H}_2\text{O} \rightarrow \text{Ti}(\text{OH})_4 + 2\text{H}_2$
- 199 3. $\text{Ti}(\text{OH})_4 + 2\text{H}_2 \rightarrow \text{TiO}_{2-x}(\text{OH})_{2-x} + (2-x)\text{H}_2\text{O}$
- 200 4. $\text{TiO}_{2-x}(\text{OH})_{2-x} + (2-x)\text{H}_2\text{O} \xrightarrow{\Delta} \text{TiO}_2 (\text{Anatase})$

201

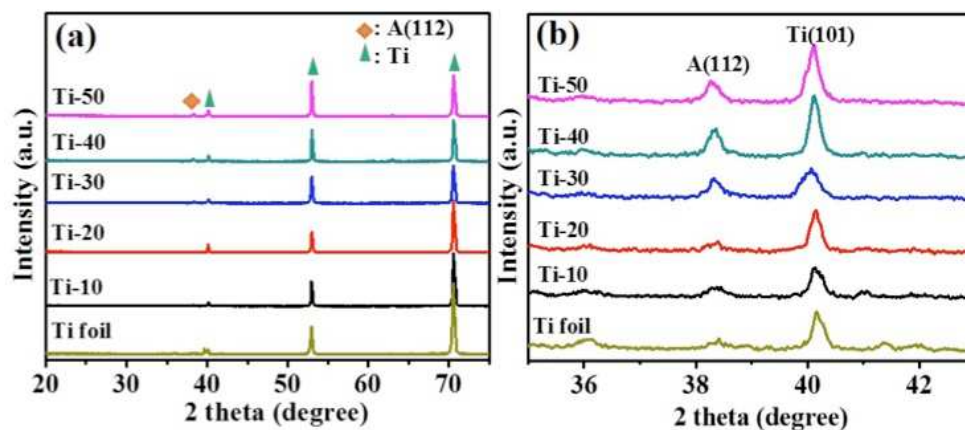
202 **Fig 3(a)** shows the XRD data of the anodized Ti foils[54]. An expanded view,
 203 **Fig. 3(b)**, allows the (112) peak to be attributed to the anatase phase of TiO_2 [1999 JCPDS-
 204 ICDD File Card #83-2243]. The intensity of the anatase (112) peak increases with current, a
 205 result in agreement with earlier studies[55].

206

207

207

208



209

210 **Fig. 3.** XRD patterns of: (a) electrochemically anodized Ti foils; and (b) partially enlarged
 211 view of the XRD patterns in the range 35-43°.

212

213 X-ray photoelectron spectroscopy (XPS) was employed to study the surface
 214 composition and electronic structure of the electrochemically anodized Ti foil samples. The
 215 high resolution XPS spectra of Ti 2p and O 1s regions of sample Ti-30, taken as a
 216 representative sample, are shown in **Fig 4(a)** and **4(b)** respectively. The two main peaks
 217 appearing at 458.57 eV and 464.31 eV are associated with Ti 2p_{3/2} and Ti 2p_{1/2} respectively,
 218 assuring the occurrence of Ti atoms in Ti⁺⁴ oxidation state. The spin orbital splitting between
 219 Ti 2p_{3/2} and Ti 2p_{1/2} signals is 5.75 eV, in excellent agreement with reported literature
 220 values[56]. A FWHM of 1.09 eV for the Ti 2p_{3/2} signal is obtained, with the binding energy
 221 difference between O 1s and Ti 2p_{3/2} calculated as 71.8 eV, parameters that well agree with
 222 the reported values of anatase TiO₂[57,58]. **Fig. 4(b)** shows the deconvoluted peaks of O 1s
 223 peak; the tail extending towards higher energies is similar to previous reports for TiO₂ anatase
 224 powder[57], nanocrystalline thin film[58] and anatase single crystal[59]. The deconvoluted O
 225 1s peaks at 530.06 eV and 531.31 eV correspond to the presence of O²⁻ in TiO₂ and to surface
 226 weakly adsorbed oxygen as OH⁻ and O⁻ respectively[47]. The difference in the binding energy

227 for these peaks of the assigned OH⁻ or O⁻ (531.3 eV) and O²⁻ is 1.20 eV, a value close to
 228 reported differences[60]. In conclusion, our XPS analysis confirms the presence of anatase
 229 TiO₂.

230

232

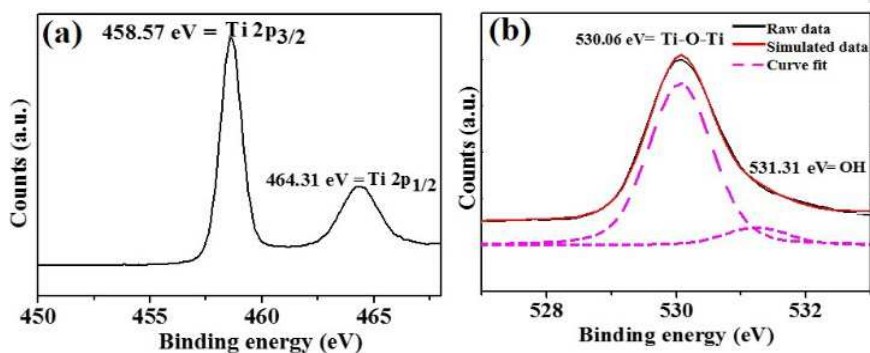
234

236

238

240

242

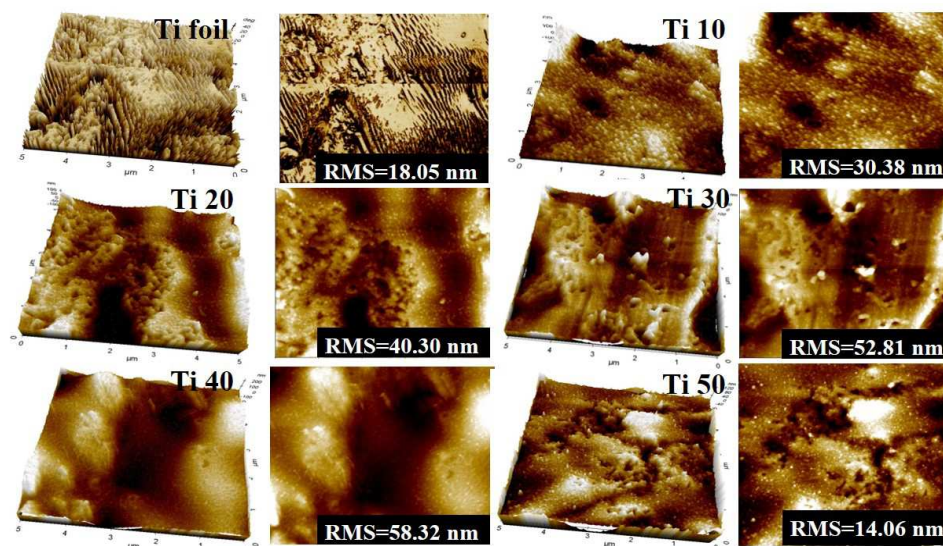


243 **Fig. 4.** X-ray photoelectron spectroscopy (XPS) of sample Ti-30 showing regions: (a) Ti 2p;
 244 and (b) O 1s.

245

246 **Fig. 5** shows three-dimensional AFM images of the anodized Ti foil surfaces. The
 247 (unanodized) Ti foil has a smooth surface with the root mean square (R_{rms}) and roughness
 248 kurtosis (R_{ku}) value of, respectively, 18.05 nm and 1.50. $R_{ku} > 3$ indicates the presence of
 249 inordinately high peaks or deep valleys, while $R_{ku} < 3$ indicates their absence [73]; the R_{ku}
 250 value for each anodized Ti foil sample was more than 3, see **Table S1** of the supplementary
 251 data. Once the anodization process is initiated the surface roughness starts increasing with a
 252 maximum value obtained for sample Ti-40. We make note that the surface roughness
 253 decreases for the Ti foil anodized at 50 mA. As discussed in the FE-SEM results, growth of
 254 the interconnected nanoweb and nanofibril networks over the Ti foil takes place via etching
 255 of the innate barrier oxide layer. However, with too large an increase in the applied current
 256 the balance between oxide formation and dissolution is disrupted, so rather than achieving a
 257 complex oxide surface topology one simply obtains a smooth, highly-etched surface[61].

258



259

260

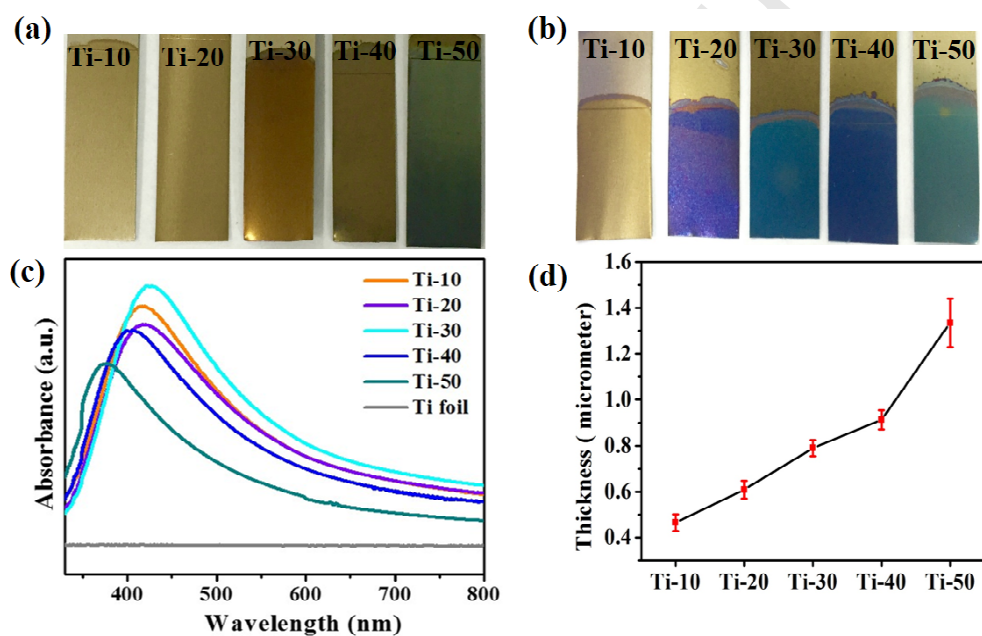
261 **Fig. 5.** AFM 3D and 2D images of the surface of electrochemically anodized Ti foils.

262

263 Digital images of electrochemically anodized Ti foil samples before and after
 264 annealing at 350°C are shown in **Fig. 6(a)** and **6(b)**, respectively; sample color is a function
 265 of oxide layer thickness [74]. **Fig. S2** and **Fig. S3** show, for two different samples prepared
 266 under the same anodization conditions, cross-sectional images of the resulting oxide layers.
 267 The thickness of oxide layer of two different samples prepared under similar conditions of
 268 electrochemical anodization is measured and the error bar representation is shown in
 269 **Fig. 6(d)**. As illustrated by the data of **Fig. 6(d)**, the oxide layer thickness increases with
 270 increasing anodization current.

271 The UV-Vis diffuse reflectance spectra of the electrochemically anodized Ti foils is
 272 shown in **Fig. 6(c)**, and the UV visible diffuse reflectance spectra of three different samples
 273 prepared under same conditions given in **Fig. S4**; the data confirms consistent absorption
 274 properties across sample sets. The samples anodized at low current values (10mA, 20mA
 275 and 30mA) show an absorbance spectrum shifted to longer wavelengths, while samples

276 anodized at higher current values (40mA and 50 mA) see a shift in their absorbance
 277 properties to shorter wavelength values. The difference in absorption of the electrochemically
 278 anodized Ti foils can be associated to the combined effects of (i) light trapping surface
 279 features, and (ii) interference oscillations induced by the oxide layer thickness. Pores are
 280 known to be responsible for better light trapping[62]; surface roughness dependent optical
 281 properties have been previously reported[63,64], with surfaces of lower roughness having
 282 lower light-absorption properties.
 283



284
 285
 286 **Fig. 6.** Digital images of electrochemically anodized Ti foils: (a) Before annealing; (b) After
 287 annealing. (c) UV-Visible DRS spectra of samples; (d) Increase in anodic oxide layer
 288 thickness with increasing applied anodization current.

289

290 3.1 Water Contact angle (WCA) measurements

291 It is well known the wettability of a solid surface is affected by surface roughness and
 292 surface composition [4, 5]. **Fig. 7** shows image illustration of WCA measurements taken for

293 anodized Ti foils in the dark and, as will be discussed momentarily, both UV and white light
294 illumination.

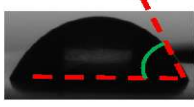
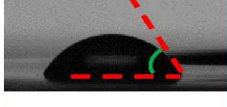
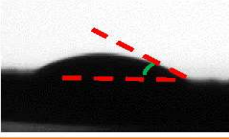
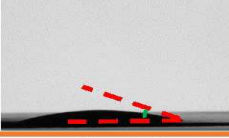
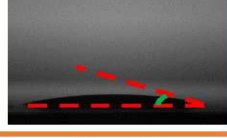
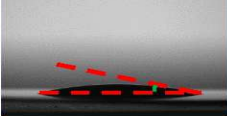
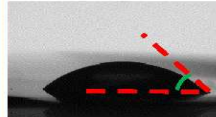
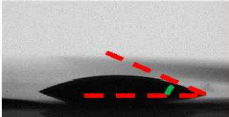
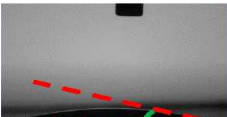
295 Under dark conditions, the Ti foil has a water contact angle of 68.1°; with anodization
296 there is a sharp decrease in the WCA for each of the anodized Ti foils although, interestingly
297 enough, Ti-40 and Ti-50 samples show little decrease in WCA, a behavior which correlates
298 with the small pore size as revealed by the FE-SEM images.

299 To evaluate the photoinduced surface wettability all samples were illuminated with
300 ultraviolet light ($\lambda = 365$ nm) using a 6 W handheld UV lamp for 5 minutes and the resulting
301 WCA measured, see **Fig. 7**. The Ti foil sample after UV illumination shows a water contact
302 angle of 65.2°. After UV illumination samples Ti-10, Ti-20 and Ti-30 became highly
303 hydrophilic, in particular sample Ti-30 which showed a WCA of 4.8°, a value considered
304 superhydrophilic[10].

305 Fig. 7 also shows the WCA of the samples upon exposure to white light. Upon
306 illumination (5 minute) the surface of Ti-10, Ti-20 and Ti-30 became highly hydrophilic, in
307 particular the sample Ti-30 which behaves as a superhydrophilic surface with a contact angle
308 less than 5°, suggesting their practical application as superhydrophilic surfaces in response to
309 indoor light. Samples Ti-40 and Ti-50, in contrast, did not show a high wettability.

310 By using measured WCA values a relationship between photoinduced hydrophilic properties
311 and surface roughness is obtained, and shown in **Fig. 8(a)** and **(b)** after, respectively, UV and
312 white light illumination.

313

Sample	Initial WCA (Under dark)	After UV illumination (5 minute)	After warm white light illumination (5 minute)
Ti foil	CA= 68° 	CA= 65.2° 	CA= 69° 
Ti 10	CA= 41.4° 	CA= 29.4° 	CA= 18.2° 
Ti 20	CA= 26.1° 	CA= 11.6° 	CA= 20° 
Ti 30	CA= 18.1° 	CA= 4.8° 	CA= 3.2° 
Ti 40	CA= 41.2° 	CA= 30.6° 	CA= 23.3° 
Ti 50	CA= 47.1° 	CA= 32.6° 	CA= 22.4° 

314

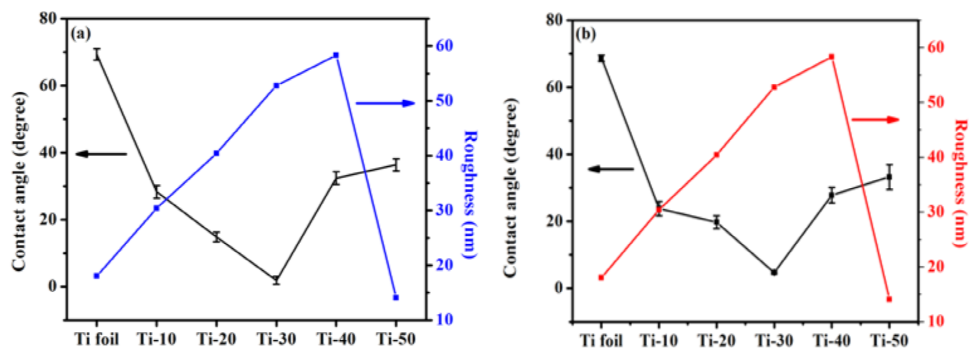
315

316 **Fig. 7.** Water contact angle (WCA) of the electrochemically anodized Ti foils in the dark,

317 after UV illumination, and after white light illumination.

318

319



320

321

322 **Fig. 8.** Change in WCA with respect to surface roughness (R_{rms}) after: (a) UV illumination;
 323 and (b) white light illumination

324

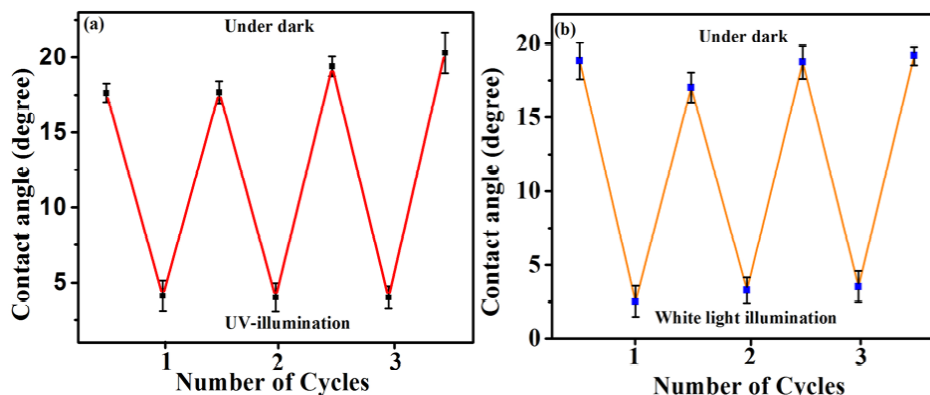
325 The anodized Ti foil samples could be repeatedly cycled through their
 326 dark/illuminated WCA values. After illumination, samples were simply dipped in DI water
 327 followed by storage in the dark; recovery is accelerated when the samples are kept on a
 328 100°C hotplate in vacuum. Such cycling can be repeated a number of times with good
 329 reproducibility, a phenomenon earlier seen for stoichiometric TiO_2 [15]. That our samples
 330 recover their initial WCA values offers the opportunity for researchers to perform
 331 experimental sets using the same sample with the same initial surface state. **Fig. 9(a)** and **(b)**
 332 shows the data for Ti-30 sample. Data for other samples is shown in **Fig. S5, S6, and S7.**

333

334

334

335



339

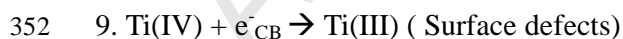
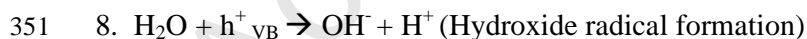
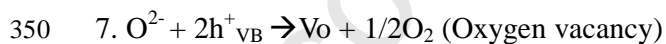
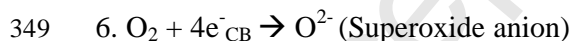
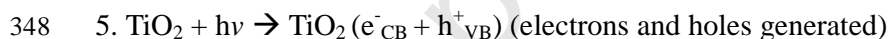
340

341 **Fig. 9.** WCA values upon repeated cycling of sample Ti-30: (a) between dark and UV light
 342 illumination; and (b) between dark and white light illumination.

343

344 XPS analysis confirms the presence of a surface-mediated OH group upon the
 345 anodized Ti foils. When the TiO₂ surface is exposed to illumination a series of reactions occur
 346 at the solid-liquid interface[45,65], which we hypothesize to be those shown in Reactions 5-9.

347



353

354 Photogenerated electrons can react with ambient oxygen to produce superoxide
 355 anions, while the positive holes (h^+) are trapped at TiO₂ lattice sites (Reaction 6 and Reaction
 356 7) [45,66–71]. These positive charges are compensated by taking electrons from the adsorbed
 357 water molecules, in turn producing hydroxyl ions (OH[·]), Reaction 8. However, a small

376 commonly used to evaluate the self-cleaning activity of photocatalytic surfaces[45]. The self-
377 cleaning properties of the electrochemically anodized Ti foils were investigated by
378 photocatalytic degradation of oleic acid ($C_{18}H_{34}O_2$), which was used as a mock organic
379 contaminant[44,45]. Results of these studies are plotted in **Fig. 11 (a)**. After the
380 contamination of electrochemically anodized Ti foils with oleic acid the samples, as
381 anticipated, exhibited a WCA of approximately 60° [72]. After irradiating the sample with
382 UV light for 25 minutes all anodized samples recovered their original state of hydrophilicity;
383 in particular sample Ti-30 showed excellent regeneration in its superhydrophilicity, see
384 **Fig. 11(b)**. For comparison, oleic acid contaminated Ti foil, illuminated under similar
385 conditions, did not show any significant change in its WCA before/after UV exposure.

386 Upon illumination an organic pollutant on a TiO_2 surface begins to photocatalytically
387 degrade, leading to a decrease in the contaminant surface coverage [15]. When this coverage
388 approaches zero a rapid spreading of water droplet occurs, see **Fig 11(a)**. As previously
389 reported, carbon dioxide and water will be formed with the photocatalytic reduction of oleic
390 acid in the presence of oxygen[45], (Reaction 10)

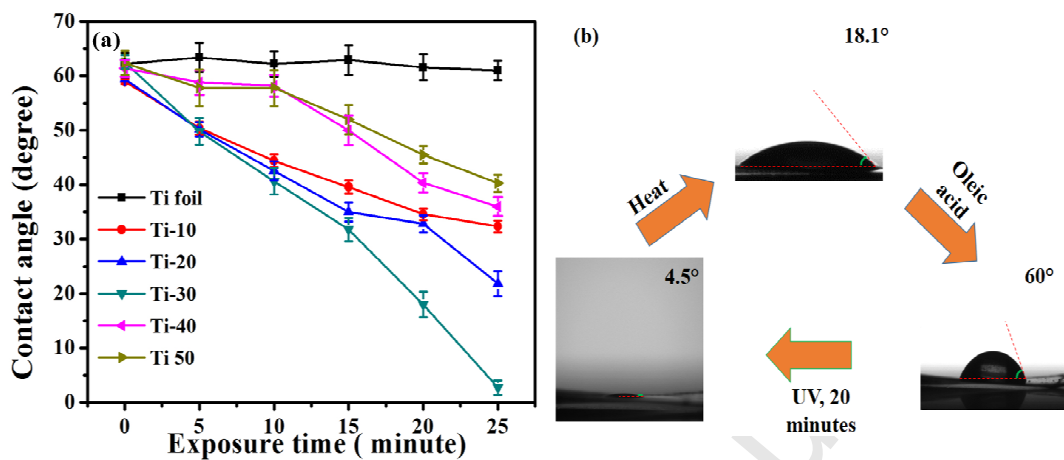
391



393

393

394



395

396

397 **Fig. 11.** (a) Time dependent change in WCA for the oleic acid contaminated samples; (b)
 398 illustration of self-cleaning process.

399

400 4. Conclusions

401 Anatase titanium dioxide films demonstrating superhydrophilic behaviour are
 402 fabricated by anodization of Ti foil substrates. As confirmed from FESEM and AFM results,
 403 an increase in anodization current leads to a change in surface topology with the formation of
 404 an interconnected nanoweb network. Sample wetting behaviour is examined for samples kept
 405 in the dark, after UV illumination, and after white light illumination. We suggest the
 406 superhydrophilic behaviour of the anodized samples, obtained after either UV or white light
 407 illumination, originates from the surface topology, chemical constitution, and light
 408 absorption. Notably, sample Ti-30 demonstrates a WCA of approximately 4.8° after UV
 409 illumination, and 3.2° after white light exposure. The surfaces exhibit effective self-
 410 cleaning/photocatalytic properties, with rapid reduction of oleic acid, our test organic
 411 contaminant, by which the superhydrophilic properties are restored. The described anodized

412 Ti foil samples show excellent reproducibility in their initial surface states after undergoing
413 repeated cycles of illumination, indicating durability of surface wettability properties.

414 We suggest the facile synthesis strategy used to obtain the superhydrophilic Ti
415 surfaces may find extensive use in applications including orthopaedic implants, and as a host
416 material of specific surface wettability characteristics used for immobilizing specific targets
417 such as biomolecules.

418

419 **Acknowledgements**

420 The authors gratefully acknowledges the support by the DGIST R&D Program of the
421 Ministry of Education, Science and Technology of Korea (16-BD-0404) and by Basic
422 Science research program through the National Research Foundation of Korea funded by the
423 Ministry of Science, ICT & Future Planning (2013R1A1A008678 &
424 2014K1A3A1A47067086). This research was also supported by the Technology
425 Development Program to Solve Climate Changes of the National Research Foundation (NRF)
426 funded by the Ministry of Science, ICT & Future Planning (2015M1A2A2074670). The
427 authors are thankful to DGIST R&D Program and MIREBrain Program of the Ministry of
428 Science, ICT & Future Planning (15-01-HRSS01 & 201510023).

429

430 **Appendix A. Supplementary data**

431 FE-SEM images of electrochemically anodized Ti foils at different conditions; Cross-
432 sectional FESEM images of TiO₂ films; Mean UV-Visible DRS spectra of three different
433 samples prepared under similar conditions; WCA of the anodized Ti foil samples showing
434 their reproducible nature; table showing roughness kurtosis values (R_{ku}) of anodized Ti foil
435 samples; tables showing average values and relative errors of WCA measurements; and
436 spectrum of white light used in experiments is available in the online version of this article.

437

438 **References**

- 439 [1] K. Liu, X. Yao, L. Jiang, *Chem. Soc. Rev.* 39 (2010) 3240–55.
- 440 [2] K. Koch, B. Bhushan, W. Barthlott, *Prog. Mater. Sci.* 54 (2009) 137–78.
- 441 [3] B.L. Feng, S.H. Li, Y.S. Li, H.J. Li, L.J. Zhang, J. Zhai, Y.L. Song, B.Q. Liu, L. Jiang,
442 D.B. Zhu, *Adv. Mater.* 14 (2002) 1857–60.
- 443 [4] R.N. Wenzel, *J. Ind. Eng. Chem.* 28 (1936) 988–94.
- 444 [5] B.D. Cassie, 5 (1944) 546–51.
- 445 [6] T. Sun, L.I.N. Feng, 38 (2005) 644–52.
- 446 [7] S. Tang, O.J. Kwon, N. Lu, H.S. Choi, *Surf. Coatings Technol.* 195 (2005) 298–306.
- 447 [8] Y. Takata, S. Hidaka, M. Masuda, T. Ito, *Int. J. Energy Res.* 27 (2003) 111–9.
- 448 [9] S. Tugulu, K. Löwe, D. Scharnweber, F. Schlottig, *J. Mater. Sci. Mater. Med.* 21
449 (2010) 2751–63.
- 450 [10] C.J. Wu, C.J. Huang, S. Jiang, Y.J. Sheng, H.K. Tsao, *RSC Adv.* 6 (2016) 24827–34.
- 451 [11] K. Hashimoto, H. Irie, A. Fujishima, *Jpn. J. Appl. Phys.* 44 (2005) 8269–85.
- 452 [12] B. Bharti, S. Kumar, R. Kumar, *Appl. Surf. Sci.* 364 (2016) 51–60.
- 453 [13] M.Y. Lan, C.P. Liu, H.H. Huang, J.K. Chang, S.W. Lee, *Nanoscale Res. Lett.* 8 (2013)
454 1–8.
- 455 [14] A. Aladjem, *J. Mater. Sci.* 8 (1973) 688–704.
- 456 [15] Z. Wu, D. Lee, M.F. Rubner, R.E. Cohen, *Small* 3 (2007) 1445–54.
- 457 [16] M. Mokhtarimehr, M. Pakshir, A. Eshaghi, M.H. Shariat, *Thin Solid Films* 532 (2013)
458 123–6.
- 459 [17] V. Veiko, M. Sergeev, G. Kostyuk, 10 (2015) 1–4.
- 460 [18] S. Hoshian, V. Jokinen, K. Hjort, R.H.A. Ras, S. Franssila, *ACS Appl. Mater.*
461 *Interfaces* 7 (2015) 15593–9.

- 462 [19] Y. Lai, F. Pan, C. Xu, H. Fuchs, L. Chi, *Adv. Mater.* 25 (2013) 1682–6.
- 463 [20] J. Huang, Y. Lai, L. Wang, S. Li, M. Ge, K. Zhang, H. Fuchs, L. Chi, *J. Mater. Chem.*
464 *A* 2 (2014) 18531–8.
- 465 [21] J.Y. Huang, Y.K. Lai, F. Pan, L. Yang, H. Wang, K.Q. Zhang, H. Fuchs, L.F. Chi, *Small*
466 10 (2014) 4865–73.
- 467 [22] Y. Lai, L. Lin, F. Pan, J. Huang, R. Song, Y. Huang, C. Lin, H. Fuchs, L. Chi, *Small* 9
468 (2013) 2945–53.
- 469 [23] G. Liu, K. Du, K. Wang, *Appl. Surf. Sci.* 388 (2016) 313–320.
- 470 [24] Y. Lai, J. Huang, Z. Cui, M. Ge, K.-Q. Zhang, Z. Chen, L. Chi, *Small* 12 (2016) 2203–
471 2224.
- 472 [25] J. Wang, H. Li, Y. Sun, B. Bai, Y. Zhang, Y. Fan, *Small* 11 (2016) 710–23.
- 473 [26] S.J. Cho, J.H. Boo, J.M. Kim, D.G. Jung, S.S. Kim, *Adv. Mater. Res.* 415 (2011) 1879–
474 82.
- 475 [27] R.S. Bedi, R. Cai, C. O’Neill, D.E. Beving, S. Foster, S. Guthrie, W. Chen, Y. Yan,
476 *Microporous Mesoporous Mater.* 151 (2012) 352–7.
- 477 [28] C. O’Neill, D.E. Beving, W. Chen, Y. Yan, *AIChE J.* 52 (2006) 1157–61.
- 478 [29] R.D. Sun, A. Nakajima, A. Fujishima, T. Watanabe, K. Hashimoto, *J. Phys. Chem. B*
479 105 (2001) 1984–90.
- 480 [30] G.K. Mor, O.K. Varghese, M. Paulose, C.A. Grimes, *Sens. Lett.* 1 (2003) 42–6.
- 481 [31] G.K. Mor, M.A. Carvalho, O.K. Varghese, M. V. Pishko, C.A. Grimes, *J. Mater. Res.*
482 19 (2004) 628–34.
- 483 [32] T. Verho, C. Bower, P. Andrew, S. Franssila, O. Ikkala, R.H.A. Ras, *Adv. Mater.* 23
484 (2011) 673–8.
- 485 [33] S. Hwangbo, J. Heo, X. Lin, C. Moonhyun, J. Hong, *Sci. Rep.* 6 (2016) 1–12.
- 486 [34] J. Yu, G. Dai, B. Cheng, *J. Phys. Chem. C* 114 (2010) 19378–85.

- 487 [35] S. Uttiya, D. Contarino, S. Prandi, M. Carnasciali, G. Gemme, L. Mattera, R. Rolandi,
488 Journal of Material Science & Nanotechnology 1 (2009) 1-8.
- 489 [36] S. Functionalization, B.D. Wiltshire, (2016) 1–6.
- 490 [37] S. Farsinezhad, P.R. Waghmare, B.D. Wiltshire, H. Sharma, S. Amiri, S.K. Mitra, K.
491 Shankar, RSC Adv. 4 (2014) 33587.
- 492 [38] X.Q. Meng, D.X. Zhao, J.Y. Zhang, D.Z. Shen, Y.M. Lu, L. Dong, Z.Y. Xiao, Y.C. Liu,
493 X.W. Fan, Chem. Phys. Lett. 413 (2005) 450–3.
- 494 [39] L.M. Chamberlain, K.S. Brammer, G.W. Johnston, S. Chien, S. Jin, J. Biomater.
495 Nanobiotechnol. 2 (2011) 293–300.
- 496 [40] T.W. Chung, D.Z. Liu, S.Y. Wang, S.S. Wang, Biomaterials 24 (2003) 4655–61.
- 497 [41] Y. Gong, S.T. Misture, P. Gao, N.P. Mellott, J. Phys. Chem. C 120 (2016) 22358–64.
- 498 [42] R.A. Ghostine, R.M. Jisr, A. Lehaf, J.B. Schlenoff, Langmuir 29 (2013) 11742–50.
- 499 [43] J.D. Miller, 36 (2015) (1996).
- 500 [44] J. Cai, J. Ye, S. Chen, X. Zhao, D. Zhang, S. Chen, Y. Ma, S. Jin, L. Qi, Energy
501 Environ. Sci. 5 (2012) 7575.
- 502 [45] S. Banerjee, D.D. Dionysiou, S.C. Pillai, Appl. Catal. B Environ. 176–177 (2015) 396–
503 428.
- 504 [46] L. Zhang, Y. Zhong, D. Cha, P. Wang, Sci. Rep. 3 (2013) 2326.
- 505 [47] H. Thissen, A. Koegler, M. Salwiczek, C.D. Easton, Y. Qu, T. Lithgow, R.A. Evans,
506 NPG Asia Mater. 7 (2015)
- 507 [48] L.C. Hsu, J. Fang, D.A.B.Tasciuc, R.W. Worobo, C.I. Moraru, Appl. Environ.
508 Microbiol. 79(8) (2013) 2703–12.
- 509 [49] A. Prusi, L. Arsov, B. Haran, B.N. Popov, J. Electrochem. Soc. 149 (2002) B491.
- 510 [50] C.Y. Chen, K. Ozasa, F. Kitamura, K.I. Katsumata, M. Maeda, K. Okada, N.
511 Matsushita, Electrochim. Acta 153 (2015) 409–15.

- 512 [51] J. Yu, G. Dai, B. Cheng, *J. Phys. Chem. C* 114 (2010) 19378–85.
- 513 [52] Y.T. Sul, C.B. Johansson, Y. Jeong, T. Albrektsson, *Med. Eng. Phys.* 23 (2001) 329–46.
- 514 [53] I. Bezares, A. D. Campo, P. Herrasti, A. M. Bonilla, *Phys. Chem. Chem. Phys.* 17
515 (2015) 29319–26.
- 516 [54] S. Berger, A. Ghicov, Y.C. Nah, P. Schmuki, *Langmuir* 25 (2009) 4841–4.
- 517 [55] M. V. Diamanti, B. D. Curto, M.P. Pedferri, *Color Res. Appl.* 33(2008) 221–8.
- 518 [56] M.C. Biesinger, B.P. Payne, A.P. Grosvenor, L.W.M. Lau, A.R. Gerson, R.S.C. Smart,
519 *Appl. Surf. Sci.* 257 (2011) 2717–30.
- 520 [57] B. Schumacher, V. Plzak, J. Cai, R.J. Behm, *Catal. Letters* 101(2005) 215–24.
- 521 [58] A. Orendorz, J. Wüsten, C. Ziegler, H. Gnaser, *Appl. Surf. Sci.* 252 (2005) 85–8. 10.
- 522 [59] R. Sanjinés, H. Tang, H. Berger, F. Gozzo, G. Margaritondo, F. Lévy, *J. Appl. Phys.* 75
523 (1994) 2945–51.
- 524 [60] B. Erdem, R. A. Hunsicker, G.W. Simmons, E.D. Sudol, V.L. Dimonie, M.S. El-aasser,
525 *Langmuir* 17 (2001) 2664–9.
- 526 [61] L. Wu, J. Liu, M. Yu, S. Li, H. Liang, M. Zhu, *Int. J. Electrochem. Sci.* 9 (2014) 5012–
527 24.
- 528 [62] M. Li, Y. Su, J. Zhao, H. Geng, J. Zhang, L. Zhang, C. Yang, Y. Zhang,
529 *CrystEngComm* 17(6) (2015) 1296–304.
- 530 [63] B. Zhao, J. Zhou, L. Rong, *Trans. Nonferrous Met. Soc. China* 20 (2010) 1429–33.
- 531 [64] F. Aousgi, W. Dimassi, B. Bessais, M. Kanzari, *Appl. Surf. Sci.* 350 (2015) 19–24.
- 532 [65] R. Wang, K. Hashimoto, A. Fujishima, M. Chikuni, E. Kojima, A. Kitamura, M.
533 Shimohigoshi, T. Watanabe, *Nature* 388 (1997) 431–2.
- 534 [66] R. Wang, K. Hashimoto, A. Fujishima, M. Chikuni, E. Kojima, A. Kitamura, M.
535 Shimohigoshi, T. Watanabe, *Adv. Mater.* 10 (1998) 135–8.
- 536 [67] N. Sakai, R. Wang, A. Fujishima, T. Watanabe, K. Hashimoto, *Langmuir* 14 (1998)

- 537 5918–20.
- 538 [68] R. Wang, N. Sakai, A. Fujishima, T. Watanabe, K. Hashimoto, *J. Phys. Chem. B*
539 103(12) (1999) 2188–94.
- 540 [69] P. V. Kamat, *J. Phys. Chem. C* 111(7) (2007) 2834–60.
- 541 [70] A. Fujishima, K. Honda, *Nature* 238 (1972) 37–8.
- 542 [71] L. Zhang, Y. Zhong, D. Cha, P. Wang, *Sci. Rep.* 3 (2013).
- 543 [72] Y. Wan, B. Sun, W. Liu, C. Qi, *J. Sol-Gel Sci. Technol.* 61(3) (2012) 558–64.
- 544 [73] Bhushan B. *Surface roughness analysis and measurement techniques*. Taylor and
545 Francis:New York, **2001**; pp 1-71.
- 546 [74] Tilley R. *Color and the Optical properties of materials*. J Wiley: Chichester, UK, **2000**;
547 pp 1-53.
- 548 [75] in: ISO 27448: 2009 Fine ceramics (advanced ceramics, advanced technical ceramics)
549 -Test method for self-cleaning performance of semiconducting photocatalytic materials
550 – Measurement of water contact angle.

551

552

553

Highlights

554

555

556

557

558

559

560

- A facile & scalable synthesis route to obtain superhydrophilic titanium surfaces.
- Electrochemical anodization of Ti foil results in nano-architected anatase TiO₂ films.
- Nanowebs and nanofibrils structures obtained over anodized Ti foil.
- Investigation of photoinduced superhydrophilic properties.
- Surfaces with enhanced light absorbance & surface roughness properties.